Learning induces neurotrophin signaling at hippocampal synapses

Lulu Y. Chen[a], Christopher S. Rex[b], Yas Sanaiha[a], Gary Lynch[a,b], and Christine M. Gall[a,c,1]

Departments of [a]Anatomy and Neurobiology, [b]Psychiatry and Human Behavior, and [c]Neurobiology and Behavior, University of California, Irvine, CA 92697

Edited* by Richard F. Thompson, University of Southern California, Los Angeles, CA, and approved February 2, 2010 (received for review November 17, 2009)

Learning-induced trophic activity is thought to be critical for maintaining health of the aging brain. We report here that learning, acting through an unexpected pathway, activates synaptic receptors for one of the brain's primary trophic factors. Unsupervised learning, but not exploratory activity alone, robustly increased the number of postsynaptic densities associated with activated (phosphorylated) forms of BDNF's TrkB receptor in adult rat hippocampus; these increases were blocked by an NMDA receptor antagonist. Similarly, stimulation of hippocampal slices at the learning-related theta frequency increased synaptic TrkB phosphorylation in an NMDA receptor–dependent fashion. Theta burst stimulation, which was more effective in this regard than other stimulation patterns, preferentially engaged NMDA receptors that, in turn, activated Src kinases. Blocking the latter, or scavenging extracellular TrkB ligands, prevented theta-induced TrkB phosphorylation. Thus, synaptic TrkB activation was dependent upon both ligand presentation and postsynaptic signaling cascades. These results show that afferent activity patterns and cellular events involved in memory encoding initiate BDNF signaling through synaptic TrkB, thereby ensuring that learning will trigger neurotrophic support.

BDNF | NMDA receptor | Src kinase | theta burst stimulation | TrkB

Environmental enrichment and learning modify brain anatomy (1) and chemistry (2, 3) in older animals and slow cognitive decline and the onset of dementia in aged humans (4). Although multiple factors likely contribute to these effects, it is generally agreed that trophic factors play a central role. These releasable peptides stimulate growth and help maintain neuronal viability (5, 6) and are logical candidates for the agency whereby experience slows age-related deterioration of brain networks (7). However, there is little evidence that learning or learning-related patterns of electrical activity actually stimulate neurotrophic signaling at brain synapses. The absence of tests of the learning/trophic signaling hypothesis is likely due to difficulties in sampling the activation state of proteins in the very small percentage of synapses affected by physiologically relevant patterns of activity or by learning itself (8, 9). Recent advances in restorative deconvolution microscopy have partly obviated these problems (8, 10). We used these techniques in the present studies to test the hypothesis that learning and learning-related brain rhythms cause the rapid activation of BDNF's TrkB receptor within synapses of the adult hippocampus.

BDNF is of particular interest with regard to experience and aging because its expression by cortical neurons is both regulated by activity (11) and related to age-associated changes in brain anatomy and functioning (12). Accordingly, we focused on BDNF and asked if a 30 min period of a ubiquitous form of mammalian learning (i.e., unsupervised learning of a novel environment) increases the number of synapses containing the activated form of TrkB (13). We also tested if, as predicted, afferent stimulation that mimics neuronal activity patterns occurring during spatial learning (14, 15) similarly activates synaptic TrkB and, if so, by what mechanism. The results confirm that learning does in fact drive trophic signaling that supports neuronal viability and provide a detailed description of how this relationship is achieved.

Results

Studies of the effects of synaptic activity on BDNF signaling employed three antisera directed against tyrosine residues that are phosphorylated (p) with Trk activation (Trk^{Y490}, TrkB^{Y515}, and TrkB^{Y816}). The TrkB^{Y515} and Trk^{Y490} residues mediate SHC binding, whereas TrkB^{Y816}, which lies within the C terminus of TrkB only, binds phospholipase C-gamma (16). Immunoprecipitation confirmed that the anti-TrkB^{Y515} does not bind detectable levels of TrkA in adult rat hippocampus (Fig. S1). Immunostaining for total TrkB was predominantly localized to small dense structures that were evenly distributed across all lamina of hippocampal field CA1 in adult male Long-Evans and Sprague-Dawley rats; labeling for pTrkB was qualitatively similar but was much less frequent. Comparable results were obtained with each of the three pTrk antisera (Fig. 1*A*). Deconvolved immunofluorescence images showed that TrkB-immunopositive (+) elements were commonly, although not ubiquitously, colabeled with antisera to the postsynaptic scaffold protein, PSD95 (Fig. 1*B*) thereby demonstrating localization to the postsynaptic element of excitatory, glutamatergic synapses.

Tests for behaviorally induced phosphorylation of TrkB used an unsupervised learning (USL) paradigm in which rats quickly acquire information about a novel, complex environment without explicit rewards (9). Adult Long-Evans rats were handled and acclimated to i.p. vehicle (VEH) injections over a period of several days. On the test day, control and experimental/USL rats were transported to the test room but only the latter were introduced into an open field containing subcompartments as well as local and distant cues (Fig. S2). The two groups (home cage control and USL) were subdivided into animals that were injected with VEH or the centrally active NMDA receptor (NMDAR) antagonist (*R*,*S*)-3-(2-carboxypiperazin-4-yl)propyl-1-phosphonic acid (CPP), the latter at concentrations that block long-term potentiation (LTP) (17) and long-term memory (9), 30 min before being transported to the test room. Rats from all groups were killed immediately after the 30 min exploration session and tissue sections from the rostral third of hippocampus were processed for immunofluorescence. An average of 8,000 synapses (labeled with anti-PSD95) per image and 500,000 synapses per rat were sampled in proximal stratum (str.) radiatum of field CA1b (Fig. S3*A*).

Only a small percentage of synapses were associated with dense immunostaining for pTrk^{Y490} (Fig. 1*C*). Blind, automated counting indicated that 5.8 ± 0.6% (mean ± SEM) of the total PSD95+ population was colabeled for pTrk in the control-VEH group (n = 12); very similar values (5.4 ± 0.7%) were obtained for control-CPP rats (n = 9), indicating that the NMDAR

Author contributions: L.Y.C., C.S.R., G.L., and C.M.G. designed research; L.Y.C., C.S.R., and Y.S. performed research; L.Y.C., C.S.R., and G.L. analyzed data; and L.Y.C., C.S.R., G.L., and C.M.G. wrote the paper.

The authors declare no conflict of interest.

*This Direct Submission article had a prearranged editor.

[1]To whom correspondence should be addressed. E-mail: cmgall@uci.edu.

This article contains supporting information online at www.pnas.org/cgi/content/full/0912973107/DCSupplemental.

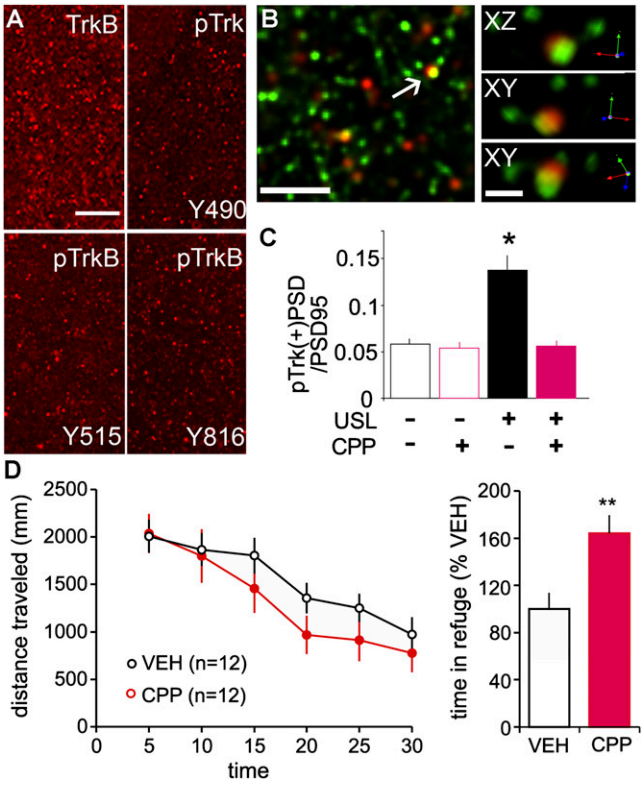

Fig. 1. Postsynaptic TrkB phosphorylation is increased with unsupervised learning. (*A*) Immunolabeling for total TrkB, pTrk^{Y490}, pTrkB^{Y515}, and pTrkB^{Y816} in CA1b str. radiatum of control Long-Evans rats (brain sections). (Scale bar: 20 μm.) (*B*) 3D reconstruction of deconvolved Z-series images show (*Left*) double immunolabeling for pTrk^{Y490} (red) and PSD95 (green) and (*Right*) one double-labeled element from linear (XY) and orthogonal (XZ) perspectives (Scale bars: 5 and 1 μm, respectively.). (*C*) Numbers of pTrkB+ PSDs, expressed as a fraction of total PSDs, for rats given 30-min USL and for yoked, untrained controls, each with and without NMDAR antagonist CPP treatment. USL rats had over two-fold more pTrkB+ synapses relative to VEH-controls; this effect was blocked by CPP (ANOVA: $P < 0.0001$; USL/no CPP: $P < 0.001$ vs. other three groups). (*D, Left*) Plot shows CPP did not change levels of exploration (distance traveled) during USL and had little effect on within-session habituation. (*Right*) Percent time spent in the complex environment darkened compartment was greater in CPP- vs. VEH-rats ($P = 0.005$). The summarized values are normalized to the mean of the VEH group for each of two cohorts of rats used.

antagonist did not affect pTrkB levels in home cage controls. Exploration resulted in a more than twofold increase in numbers of double-labeled synapses: in USL-VEH rats (n = 12) 13.7 ± 2.0% of the total PSD95+ population was pTrk immunoreactive (Fig. 1*C*). The dramatic increase in numbers of pTrk+ postsynaptic densities (PSDs) in VEH-treated USL animals was altogether absent in CPP-treated USL rats (5.6 ± 0.6%) (ANOVA: $P < 0.0001$; $P < 0.001$ for USL-VEH rats vs. the three remaining groups; $P > 0.05$ for all other comparisons).

Behavioral measures showed that CPP tended to decrease distance traveled during the 30 min test session but this did not reach statistical significance (P = 0.08). The rate of habituation across the 30 min trial appeared normal but there was an increase in percent time spent in the darkened compartment (Fig. 1*D*). Despite its relatively modest effects during day 1, CPP caused a clear impairment in long-term memory on day 2 testing, as shown previously (9).

The above results demonstrate that unsupervised learning, but not motor activity alone, is associated with marked, NMDA receptor-dependent increases in synaptic TrkB phosphorylation. Unsupervised exploration is accompanied by extended bouts of theta frequency activity (burst discharges, EEG) in hippocampus and cortex, and there is a sizeable body of evidence suggesting that this activity is critical for the encoding of stable memory (18). We therefore tested if theta burst stimulation (TBS) activates TrkB receptors as a first step in uncovering the mechanisms underlying the above effects of learning.

In slices from adult Sprague-Dawley rats, a single train of 10 theta bursts (40 pulses over 2 s) was delivered to the Schaffer-commissural projections within hippocampal field CA1 thereby inducing synaptic potentiation (LTP) (Fig. 2*A*) and pTrk+ PSDs were quantified in the dendritic sublamina containing the stimulated synapses. TBS significantly increased pTrk^{Y490}+ puncta colocalized with PSD95 at 7 min post-TBS (P = 0.001) (Fig. 2*C*) but had no effect on total numbers of PSD95+, TrkB+, or pTrk^{Y490}+ puncta (Fig. 2*B*) indicating a predominant effect in the postsynaptic compartment versus other TrkB loci (e.g., lipid rafts). TBS-induced increases in synaptic pTrk levels were also found with antisera against pTrkB^{Y515} and pTrkB^{Y816} (Fig. 2*C*) and were restricted to the lamina (proximal str. radiatum) containing stimulated afferents as there were no changes in numbers of pTrk^{Y490}+ PSDs in the more distal dendritic field (con vs. TBS: 0.80 ± 0.16 vs. 0.71 ± 0.01/100 μm^3 for str. lacunosum/moleculare, n = 6/group).

We next used local infusions of the membrane-impermeable TrkB ligand scavenger TrkB-Fc (2 μg/mL; 30 min) or the control IgG-Fc to test if extracellular neurotrophins are responsible for the activity-induced increases in postsynaptic Trk phosphorylation. Infusion of TrkB-Fc did not alter baseline physiology or

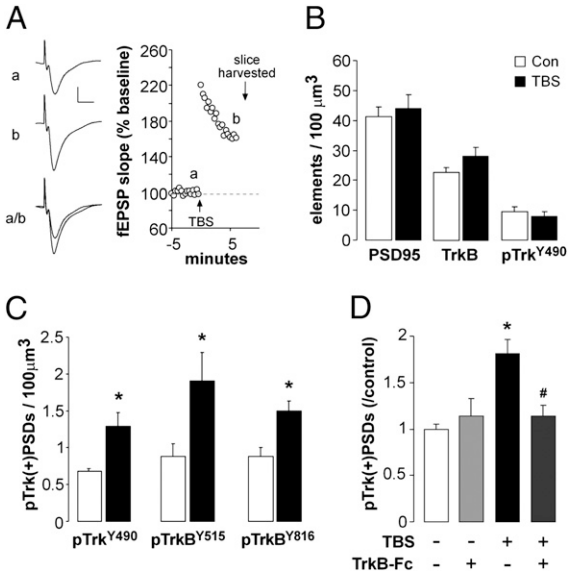

Fig. 2. LTP is associated with increases in postsynaptic pTrkB. Slices from adult Sprague-Dawley rat hippocampus received TBS or control (con) stimulation to Schaffer collateral projections and were harvested for immunofluorescence 7 min later. (*A*) Traces (*Left*) and plot of field EPSP slopes (*Right*) obtained during (*a*) baseline recording and (*b*) immediately before slice harvest from a representative experiment. (*B*) Graph shows the mean (± SEM) numbers of PSD95+, TrkB+, and pTrk^{Y490}+ puncta (irrespective of double labeling) in slices that received TBS or con stimulation: No effect of stimulation was observed ($P > 0.5$, two-tailed t test; n = 10/group). (*C*) Plot of the numbers of pTrk/PSD95 double-immunopositive elements [pTrk(+)PSDs] in CA1 str. radiatum in separate experiments using antisera to Trk^{Y490}, TrkB^{Y515}, or TrkB^{Y816}. TBS increased numbers of pTrk(+)PSDs in each case (*$P < 0.05$ vs. Con; n = 6/group). (*D*) TrkB-Fc (2 μg/mL) applied to slices beginning 30 min before TBS blocked the effect of stimulation on pTrk^{Y490} in the postsynaptic compartment (i.e., colocalized with PSD95): graph shows counts of double-labeled elements normalized to paired control values (*P = 0.0002 vs. con, #P = 0.011 vs. TBS alone, n = 6–8/group).

the initial expression of LTP but it completely blocked TBS-induced increases in synaptic Trk phosphorylation; IgG-Fc had no effect (Fig. 2*D*). These results indicate that the induction conditions for LTP are associated with a synapse-specific, BDNF-dependent increase in TrkB phosphorylation.

To determine if the learning-related theta burst activity is particularly potent for engaging BDNF signaling, we compared TBS with other stimulation patterns containing the same number of pulses: (*i*) single pulses (0.05 Hz; control stimulation), (*ii*) conventional TBS (as above), (*iii*) low-frequency bursts (LFB) (ten 100 Hz four-pulse bursts separated by 1 s), or (*iv*) a single 100 Hz high frequency train (HFS). Control and LFB stimulation produced little or no potentiation, and LTP generated by HFS was significant but smaller than that obtained with TBS ($P < 0.05$; assessed 30–40 min after stimulation) (Fig. 3*A*). Slices harvested 7 min after each stimulation regimen were processed for dual PSD95 and pTrk^{Y490} immunofluorescence. Counts of double-labeled puncta showed that TBS caused a greater increase in pTrk+ synapses than did HFS ($P = 0.012$) whereas LFB had no detectable effect ($P < 0.01$ vs. either HFS or TBS; Fig. 3*B*).

Theta burst stimulation could gain greater potency for TrkB phosphorylation, relative to other stimulation patterns, through differential effects on BDNF release or on the postsynaptic machinery that induces LTP. In accord with the latter, we found that the NMDAR antagonist (2R)-amino-5-phosphonovaleric acid (APV) completely blocks TBS-driven Trk phosphorylation (Fig. 3*C*). TBS might therefore be more effective in activating TrkB because it has the greatest effect on NMDARs. We tested this idea by comparing APV-sensitive components of the complex synaptic responses elicited by the different stimulation patterns. APV caused only minor changes to composite field excitatory postsynaptic potentials (fEPSPs) associated with LFB but significantly reduced the second and subsequent burst responses generated by TBS and the later (greater than 100 ms) responses to HFS (Fig. 3*D*). To quantify these effects, we calculated cumulative voltage responses (mV•ms) during TBS (five bursts) and HFS in the presence and absence of APV (Fig. 3*E*). Plotting the data on a pulse-by-pulse basis (Fig. 3*F*) showed that TBS is more effective than HFS at generating progressively larger synaptic potentials with correspondingly larger NMDAR-dependent components ($P = 0.02$).

Src family kinases are likely mediators of NMDAR contributions to TrkB phosphorylation: they are concentrated in spines, engaged by NMDARs (19), and can effect TrkB transactivation (20). However, it is not known if brief episodes of TBS are sufficient to trigger synaptic Src signaling or if Src contributes to ligand-dependent TrkB activation. We found that immunoreactivities for Src and the less abundant pSrc^{Y418} (phosphorylated at the kinase activation site; Fig. S4) are punctate with a more than 40% overlap with PSD95 immunoreactivity (Fig. 4*A*). TBS significantly increased numbers of pSrc+ PSDs in field CA1 in an NMDAR-dependent fashion (Fig. 4*B*), a result that

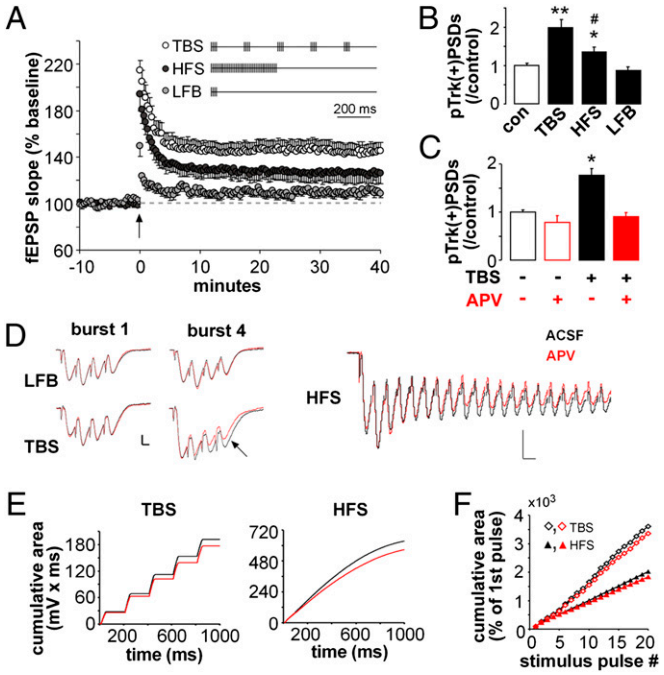

Fig. 3. Theta burst stimulation is preferentially effective for increasing spine pTrk. (*A*) Plot shows potentiation resulting from 40 stimulation pulses delivered by patterns schematized (TBS, HFS, LFB; n = 5–7/group). (*B*) Numbers of pTrk+ excitatory synapses (also PSD95+) following control (con) or patterned stimulation (*P = 0.01, **$P < 0.0001$ vs. con; #P = 0.01 vs. TBS; n = 12/group). (*C*) TBS-driven increases in pTrk(+) PSDs are blocked by the NMDAR antagonist APV (*$P < 0.001$ vs. con; n = 6/group). (*D*) TBS, LFB (*Left*), and HFS (*Right*) response traces in the presence (red) and absence (black) of APV. Calibration: 0.5 mV, 5 ms (*Left*); 0.5 mV, 10 ms (*Right*). (*E*) Cumulative area under the response-curve across 1 s TBS (20 pulses, 5 bursts) or HFS (100 pulses) with and without APV present. (*F*) Plot shows the cumulative area of responses to individual pulses (10 ms following each pulse) in the TBS and HFS trains shown in *E*. Values are expressed as percent of the fEPSP elicited by the first stimulation pulse: TBS produced significantly greater facilitation and APV-sensitive components across the duration of the trains. Plots show means ± SEM.

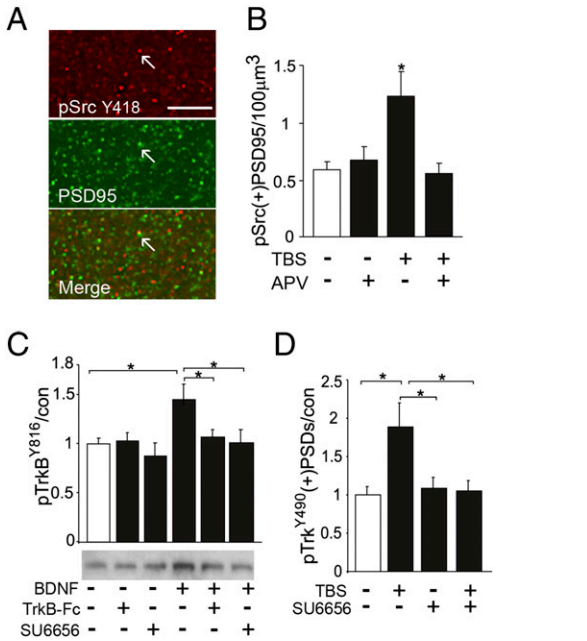

Fig. 4. TBS-driven increases in spine pTrkB are Src-dependent. (*A*) Images show pSrc^{Y418} (red), PSD95 (green), and overlapped immunolabeling in CA1 str. radiatum (yellow shows colocalization in Merge, arrows). (Scale bar: 10 µm.) pSrc^{Y418} immunoreactivity is punctate and concentrated in postsynaptic elements. (*B*) Numbers of pSrc^{Y418} and PSD95 double-immunolabeled [pSrc(+) PSD95] puncta in str. radiatum of hippocampal slices that received TBS or control stimulation, with and without 50 µM APV in the tissue bath. The pSrc+ synapses were more numerous in TBS than control slices (*P = 0.01 two-tailed t test; n = 6/group) and this effect was blocked by APV. (*C*) Representative Western blot and quantification of band densities shows that BDNF (5 min, 60 ng/mL) applied to synaptoneurosomes prepared from the adult forebrain increased levels of pTrkB^{Y816} immunoreactivity; cotreatment with Src antagonist SU6656 (20 µM) or TrkB-Fc (2 µg/mL) blocked this effect (*$P < 0.05$, n = 8/group). (*D*) Plot shows that in hippocampal slices 30 min infusion of SU6656 blocked increases in pTrk(+)PSDs normally present in slices collected 7-min post-TBS (*$P < 0.05$, n = 6–9/group).

establishes an essential condition for a synaptic TBS-NMDAR-Src-TrkB cascade.

We further explored Src involvement in ligand-dependent activation of synaptic TrkB using both synaptoneurosomes and hippocampal slices. Although Src has been shown to transactivate TrkB in the absence of ligand binding in different preparations (20, 23), the present study tested whether the kinase is also required for ligand-dependent activation. Synaptoneurosomes (21) from young adult rat forebrain were incubated with BDNF (60 ng/mL, 5 min) in the presence of VEH, the Src inhibitor SU6656, or the TrkB scavenger TrkB-Fc (22). The neurotrophin caused a marked increase in pTrkB that was completely blocked by either the Src inhibitor or the TrkB-Fc (Fig. 4*B*). In hippocampal slices, SU6656 completely blocked the twofold increase in $pTrk^{Y490}$+ PSDs produced by TBS in VEH-treated slices (Fig. 4*C*) without affecting basal levels of the phosphoprotein ($P > 0.5$). Combined with results described above, these findings indicate that TBS-induced TrkB activation is a conjoint event, involving both ligand binding and NMDAR-to-Src signaling.

Discussion

The present study constitutes a direct test of the hypothesis that learning drives synaptic trophic signaling in adult brain. We show a single 30 min episode of unsupervised learning, which is known (24) to cause pronounced and lasting changes to behavior, doubled the number of pTrkB+ synapses above values in control rats. The NMDAR antagonist CPP eliminated these increases without reducing movement within the open field, thereby indicating that extensive amounts of exploratory behavior alone do not measurably increase the phosphorylation of synaptic TrkB. Although impressive as a percentage change, increases in the learning group involved only a very small fraction of the total synaptic population, a result consistent with the broadly held assumption, necessitated by the great capacity of memory, that even substantial amounts of learning modify relatively few synapses (25). Extensive learning may, therefore, be needed to ensure that activity-driven trophic signaling extends to a substantial portion of the synaptic population and is sufficient to influence cell survival and functional integrity.

We used learning of a complex environment in these studies because it is critically dependent upon the hippocampus (26) and closely related to human behavior. It is also associated with theta bursting neuronal activity in field CA1 (15, 18), an activity pattern that is easily reproduced in slices where it produces the learning-related LTP effect (27). These features opened the way to an analysis of mechanisms that would not be possible in vivo. Using acute hippocampal slices, we found that a single train of TBS delivered to field CA1 afferents produced a large, lamina-specific increase in postsynaptic elements associated with dense pTrkB. The magnitude of this effect was as expected given the small percentage of CA1 synapses affected by conventional stimulation protocols (8, 10).

The absence of large numbers of pTrkB+ synapses in control slices or CPP-treated animals engaged in open field exploration suggests that spontaneous BDNF release is not sufficient for broad activation of synaptic TrkB (see also ref. 28). It thus appears that unusual activity is needed to initiate synaptic BDNF signaling. This raises the question of whether it is the amount or pattern of activity that engages synaptic TrkB. We found that a constant number of stimulation pulses produced a much greater effect when applied as TBS than in other formats, including the 100-Hz HFS often used to induce LTP. Together, these results, from slices and behaving rats, accord with reports that theta bursting (i.e., high frequency bursts at 100- to 200-ms interburst intervals) are evident during sampling of learning cues but are otherwise infrequent in behaving rats (15) and confirm that the brain rhythms preferentially engaged during memory encoding also set in motion cellular responses related to neuronal growth and viability.

Finally, the dependence of BDNF/TrkB signaling on select patterns of afferent activity has important implications for the role played by trophic interactions in brain aging. Historically, work in this area has focused on whether and to what degree failures in the components of neurotrophin expression might account for the neuronal atrophy that comes with aging or age-related diseases. The results for BDNF have been ambiguous; reduced expression is reported to occur in Alzheimer's (29), but it is not clear if this happens with normal aging. TrkB levels moderately decline with age in hippocampus (29), and there is evidence from transgene experiments that the receptors are needed to maintain normal spine morphology in adulthood and old age (30). Negative consequences stemming from TrkB losses could, from the present results, be exacerbated by age-related declines in theta. EEG power in the theta range, as measured during various cognitive challenges, decreases markedly with aging in humans (14). The reasons for this are unclear but are likely to generalize across mammals as age-related losses of theta are also observed in rats (31). One possibility lies in the atrophy of the cholinergic neurons in basal forebrain; these cells regulate rhythmic oscillations throughout the cortical telencephalon and are reported to atrophy with age in various species, including man (7). It remains to be seen if, as predicted from the present results, these effects lead to a loss of synaptic TrkB activation with aging and whether treatments that enhance theta reverse such declines. In any event, the results reported here suggest a mechanistic basis for arguments that learning-related behaviors, and brain activity patterns, can slow age-related deterioration of cortical operations.

Materials and Methods

All animal procedures were conducted in accordance with the National Institutes of Health Guide for the Care and Use of Laboratory Animals and with protocols approved by the Institutional Animal Care and Use Committee of the University of California, Irvine, CA. This includes efforts to minimize animal suffering and numbers of rats used.

Unsupervised Learning Paradigm and Behavioral Recordings. Procedures were slightly modified from published work (9). Briefly, the USL behavioral box (45.7 × 91.4 cm floor area; 40.6 cm high walls with an open top) included a large open field that was divided into seven subzones and a closed-top dark compartment (one fifth of total space) accessible by a small entrance (9) (Fig. S2). Rats' movements in the USL box were digitally recorded using an overhead CCD camera (WV-BP334; Panasonic) and processed using EthoVision XT video tracking software (Noldus). Discrete movements were identified as motion with initiating velocity greater than 9 cm/s and sustained velocity greater than 1 cm/s. Pauses were identified as motion less than 1 cm/s. The overall total number and duration of movements were also measured.

Six-week-old male Long-Evans rats (Harlan Labs) were handled and received daily i.p. VEH (0.9% saline) injections for 4 days before experimental use. On the fifth day, 3-(2-carboxypiperazin-4-yl)propyl-1-phosphonic acid (CPP, 10 mg/kg in saline) or VEH was injected i.p. 30 min before transport to the USL box or back to the home cage for 30 min. Immediately following this, rats were anesthetized with fluorothane gas and decapitated. Brains were rapidly removed, frozen into 2-methylbutane (−55 °C) and stored at −80 °C. Brains were cryostat sectioned coronally at 20 μm and mounted onto cold (−20 °C) slides and slowly warmed to room temperature, fixed in cold methanol (−20 °C, 10 min) and stored at −20 °C. Tissue was processed for immunofluorescence as described below.

Slice Preparation and Electrophysiology. Acute transverse hippocampal slices (350 μm) were prepared on a Leica vibroslicer from 4- to 6-week-old male Sprague-Dawley rats (Harlan Labs) (32), collected into cold artificial cerebral spinal fluid (ACSF) containing (in nM) 124 NaCl, 3 KCL, 1.25 KH_2PO_4, 2.5 $MgSO_4$, 3.4 $CaCl_2$, 26 $NaHCO_3$, and 10 dextrose, and maintained in an interface recording chamber with constant ACSF perfusion (60-70 mL/h, 32 °C) and oxygenation (95% O_2/ 5% CO_2). Electrophysiology and drug treatments were initiated 1–2 h after slice preparation.

fEPSPs were elicited by two twisted nichrome wire (65 μm) stimulation electrodes placed in str. radiatum of CA1a and CA1c to activate apical Schaffer collateral projections and were recorded with a glass pipette electrode in CA1b (32, 33). Single pulse baseline stimulation (0.05 Hz) was conducted with current intensity adjusted to generate an fEPSP with 50% of the maximum, spike-free fEPSP amplitude. The fEPSP slopes (10–90% falling phase) were measured from digitized traces (NacGather 2.0; Theta Burst Corp.). For studies involving patterned or control stimulation, slices received test stimulation (specified in main text), and synaptic responses to low frequency test pulses (3/min) were recorded until slice harvest into cold 4% paraformaldehyde in 0.1 M sodium phosphate buffer (PB). The fixed slices were sectioned at 20 μm on a freezing microtome and the slide mounted tissue was processed for immunofluorescence as described (8). Group differences in LTP were assessed by repeated measures ANOVA using SPSS software. N values represent slices/group.

Cumulative areas of responses to stimulus trains (Fig. 3*E*) were calculated as the area (mV•ms) under the curve for the specified duration of the train. Cumulative pulse area (Fig. 3*F*) was calculated as the sum of the areas under the curve of each pulse and expressed as a percentage of the area of the first pulse in the train.

Drug Treatment to Slices. Stock APV (Sigma) or SU6656 (Sigma) was prepared in dimethyl sulfoxide (<0.05% final concentration) and stored at −20 °C. Stocks were diluted in ACSF on the day of testing and bath-applied to slices for more than 30 min before testing. For within-slice stimulus train comparisons (i.e., TBS vs. HFS), slices were tested in the presence of APV first to prevent synaptic potentiation; ACSF-alone tests were conducted following more than 1-h washout. TrkB-Fc or control IgG-Fc (R&D Systems) were prepared in Tris-buffered saline containing 0.1% BSA, diluted to working concentrations in ACSF, and delivered to slices via local pipette as described (32).

Immunofluorescence. Sections to be compared were processed simultaneously for double immunofluorescence using mixtures containing anti-mouse and anti-rabbit primary antibodies (24 h, room temperature) in diluent (0.3% Triton X, 4% BSA in 0.1 M PB). Sections were then rinsed in PB and incubated with Alexa594 anti-rabbit IgG and Alexa488 anti-mouse IgG (8). Control sections were processed through all procedures with individual primary antisera omitted from the first incubation. Antibodies used included mouse anti-PSD95 (1:1,000; Affinity Bioreagents, #MA1-045) and rabbit antisera to pTrk^{Y490} (1:200; Cell Signaling, #9141), pTrkB^{Y515} (1:200; Abcam, #ab51187-100), pTrkB^{Y816} (1:200; #18664–110207-4; a gift from M. Chao, New York University, New York, NY) (16), TrkB (1:500; BD Biosciences, #611641), pSrc (1:1,000; Biosource, #44–656), Src (1:1,000; Abcam, #ab32102) and BDNF (1:1400; Biosensis, #R-088-100). Although anti-pTrk^{Y490} recognizes a site conserved across Trks A, B, and C, TrkA is not normally expressed by hippocampal neurons (34) and both neurotrophin 3 and nerve growth factor (ligands for TrkC and TrkA, respectively) are not present in the stimulated Schaffer/commissural axons (11, 35) and are therefore unlikely to contribute to results. The anti-pTrkB^{Y816} does not cross react with TrkA and has minor cross-reactivity with TrkC (16).

Imaging and Quantitative Analysis. Immunolabeled tissue sections were examined using a Leica DM6000 epifluorescence microscope with a 63× PlanApo objective (NA 1.4). Analyses were carried out on three to five tissue sections per slice within the depth range of physiological recording and between the two stimulation electrodes in mid proximo-distal str. radiatum. For each tissue section, digital images were collected using a CCD camera (ORCA-ER, Hamamatsu) at 0.2-μm focal steps to obtain a 136 × 105 × 3-μm sample. Images were processed for restorative deconvolution (Volocity 4.0, Improvision) using point-spread functions derived from a 3D reconstruction of tetraspeck fluorescent microspheres (Invitrogen) applied to experimental tissue. In-house built software was used to identify immunolabeled elements and to quantify the numbers, volumes, label intensities, and locations of immunoreactive puncta within the size parameters of dendritic spines (8, 10, 32, 33). Element boundaries were used to assess overlap between the different labels; elements were considered colabeled if any overlap between their respective boundaries was observed in 3D. Counts of immunolabeled puncta from each of the serial sections were averaged to produce a representative value for each slice.

Synaptoneurosome and Western Blot Analysis. Viable synaptoneurosomes were prepared from forebrain of male Sprague-Dawley rats (14-21 days old) as described (21). The final synaptoneurosome sample protein levels were measured (BioRad Protein Assay) and adjusted to 1.5–2 mg/mL using ACSF. All procedures before treatment were conducted at 4 °C. Synaptoneurosomal fractions were brought to room temperature and then incubated (with agitation) for 5 min with BDNF (60 ng/mL; #GF029; Millipore), SU6656 (20 μM), chimera human TrkB-Fc (1 μg/mL, T8694; Sigma), or ACSF/VEH. To test if SU6656 or TrkB-Fc blocks the effects of BDNF, samples were preincubated with inhibitors 5 min before and during BDNF treatment. Reactions were terminated by the addition of SDS-polyacrylamide gel electrophoresis sample buffer (21). Samples were processed for Western blot analysis using 8% SDS polyacrylamide gel electrophoresis; rabbit antisera to pTrkB^{Y816} (see above), TrkA or TrkB (#06–574 or #07–225; Millipore); and the ECL Plus chemiluminescence kit (Amersham) for band localization. Immunoreactive bands were measured using ImageJ (National Institutes of Health). N values represent numbers of samples tested.

Statistics. Two-tailed *t* tests and ANOVAs followed by Tukey's HSD posthoc test were used to assess significant effects between treatment groups using SPSS software.

ACKNOWLEDGMENTS. The authors thank Dr. Moses Chao for providing TrkB^{Y816} antisera, Dr. Devin Binder for helpful discussions, Anita Y. Chen for artwork, and Danielle Pham for technical support. This work was supported by National Institute of Neurological Disorders and Stroke Grant NS45620 to C.M.G. and G.L., National Institute of Mental Health Fellowship MH083396 to L.Y.C., and National Institute of Neurological Disorders and Stroke Grant NS045540 to C.S.R.

1. Faherty CJ, Kerley D, Smeyne RJ (2003) A Golgi-Cox morphological analysis of neuronal changes induced by environmental enrichment. *Brain Res Dev Brain Res* 141: 55–61.
2. Frick KM, Stearns NA, Pan JY, Berger-Sweeney J (2003) Effects of environmental enrichment on spatial memory and neurochemistry in middle-aged mice. *Learn Mem* 10:187–198.
3. Segovia G, Del Arco A, de Blas M, Garrido P, Mora F (2008) Effects of an enriched environment on the release of dopamine in the prefrontal cortex produced by stress and on working memory during aging in the awake rat. *Behav Brain Res* 187:304–311.
4. Sando SB, et al. (2008) Risk-reducing effect of education in Alzheimer's disease. *Int J Geriatr Psychiatry* 23:1156–1162.
5. Marini AM, Jiang H, Pan H, Wu X, Lipsky RH (2008) Hormesis: A promising strategy to sustain endogenous neuronal survival pathways against neurodegenerative disorders. *Ageing Res Rev* 7:21–33.
6. Mattson MP, Maudsley S, Martin B (2004) A neural signaling triumvirate that influences ageing and age-related disease: Insulin/IGF-1, BDNF and serotonin. *Ageing Res Rev* 3:445–464.
7. Nagahara AH, et al. (2009) Long-term reversal of cholinergic neuronal decline in aged non-human primates by lentiviral NGF gene delivery. *Exp Neurol* 215:153–159.
8. Chen LY, Rex CS, Casale MS, Gall CM, Lynch G (2007) Changes in synaptic morphology accompany actin signaling during LTP. *J Neurosci* 27:5363–5372.
9. Fedulov V, et al. (2007) Evidence that long-term potentiation occurs within individual hippocampal synapses during learning. *J Neurosci* 27:8031–8039.
10. Rex CS, et al. (2009) Different Rho GTPase-dependent signaling pathways initiate sequential steps in the consolidation of long-term potentiation. *J Cell Biol* 186:85–97.
11. Gall CM, Lauterborn JC (2000) Regulation of BDNF expression: Multifaceted, region-specific control of a neuronal survival factor in the adult CNS. *Neurobiology of the Neurotrophins*, ed Mocchetti I (FP Graham Publishing Co., Johnson City, TN), pp 541–579.
12. Schaaf MJ, et al. (2001) Correlation between hippocampal BDNF mRNA expression and memory performance in senescent rats. *Brain Res* 915:227–233.
13. Lu B, Pang PT, Woo NH (2005) The yin and yang of neurotrophin action. *Nat Rev Neurosci* 6:603–614.
14. Klimesch W (1999) EEG alpha and theta oscillations reflect cognitive and memory performance: A review and analysis. *Brain Res Brain Res Rev* 29:169–195.
15. Otto T, Eichenbaum H, Wiener SI, Wible CG (1991) Learning-related patterns of CA1 spike trains parallel stimulation parameters optimal for inducing hippocampal long-term potentiation. *Hippocampus* 1:181–192.
16. Arévalo JC, et al. (2006) Cell survival through Trk neurotrophin receptors is differentially regulated by ubiquitination. *Neuron* 50:549–559.
17. Abraham WC, Mason SE (1988) Effects of the NMDA receptor/channel antagonists CPP and MK801 on hippocampal field potentials and long-term potentiation in anesthetized rats. *Brain Res* 462:40–46.
18. Buzsáki G (2005) Theta rhythm of navigation: Link between path integration and landmark navigation, episodic and semantic memory. *Hippocampus* 15: 827–840.
19. Xu J, et al. (2008) Control of excitatory synaptic transmission by C-terminal Src kinase. *J Biol Chem* 283:17503–17514.
20. Rajagopal R, Chao MV (2006) A role for Fyn in Trk receptor transactivation by G-protein-coupled receptor signaling. *Mol Cell Neurosci* 33:36–46.

21. Bernard-Trifilo JA, et al. (2005) Integrin signaling cascades are operational in adult hippocampal synapses and modulate NMDA receptor physiology. *J Neurochem* 93: 834–849.
22. Blake RA, et al. (2000) SU6656, a selective src family kinase inhibitor, used to probe growth factor signaling. *Mol Cell Biol* 20:9018–9027.
23. Huang YZ, Pan E, Xiong ZQ, McNamara JO (2008) Zinc-mediated transactivation of TrkB potentiates the hippocampal mossy fiber-CA3 pyramid synapse. *Neuron* 57: 546–558.
24. Lever C, Burgess N, Cacucci F, Hartley T, O'Keefe J (2002) What can the hippocampal representation of environmental geometry tell us about Hebbian learning? *Biol Cybern* 87:356–372.
25. Granger R, Whitson J, Larson J, Lynch G (1994) Non-Hebbian properties of long-term potentiation enable high-capacity encoding of temporal sequences. *Proc Natl Acad Sci USA* 91:10104–10108.
26. Moser E, Moser MB, Andersen P (1993) Spatial learning impairment parallels the magnitude of dorsal hippocampal lesions, but is hardly present following ventral lesions. *J Neurosci* 13:3916–3925.
27. Larson J, Lynch G (1986) Induction of synaptic potentiation in hippocampus by patterned stimulation involves two events. *Science* 232:985–988.
28. Kuczewski N, et al. (2008) Backpropagating action potentials trigger dendritic release of BDNF during spontaneous network activity. *J Neurosci* 28:7013–7023.
29. Tapia-Arancibia L, Aliaga E, Silhol M, Arancibia S (2008) New insights into brain BDNF function in normal aging and Alzheimer disease. *Brain Res Rev* 59:201–220.
30. von Bohlen und Halbach O, Minichiello L, Unsicker K (2008) TrkB but not trkC receptors are necessary for postnatal maintenance of hippocampal spines. *Neurobiol Aging* 29:1247–1255.
31. Abe Y, Toyosawa K (1999) Age-related changes in rat hippocampal theta rhythms: a difference between type 1 and type 2 theta. *J Vet Med Sci* 61:543–548.
32. Rex CS, et al. (2007) Brain-derived neurotrophic factor promotes long-term potentiation-related cytoskeletal changes in adult hippocampus. *J Neurosci* 27:3017–3029.
33. Kramár EA, Lin B, Rex CS, Gall CM, Lynch G (2006) Integrin-driven actin polymerization consolidates long-term potentiation. *Proc Natl Acad Sci USA* 103:5579–5584.
34. Gibbs RB, Pfaff DW (1994) In situ hybridization detection of trkA mRNA in brain: distribution, colocalization with p75NGFR and up-regulation by nerve growth factor. *J Comp Neurol* 341:324–339.
35. Binder DK, Routbort MJ, McNamara JO (1999) Immunohistochemical evidence of seizure-induced activation of trk receptors in the mossy fiber pathway of adult rat hippocampus. *J Neurosci* 19:4616–4626.